SPANDIDOS PUBLICATIONS

ONCOLOGY REPORTS 56: 193, 2026

SGPP1 as a tumor suppressor in esophageal squamous cell carcinoma: Potential molecular mechanisms involving UGT1A9/UGT2B28 and clinical prognostic significance

LINLIN SU[1*], LIUBING HOU[1,2*], XUETAO HAN[1,3*], GE ZHANG[1], JIAYUAN LI[1], YU WANG[1], YUXIN HAN[1], XIAOYING XUE[1,3*] and HUANDI ZHOU[1-3*]

[1]Department of Radiotherapy, The Second Hospital of Hebei Medical University, Shijiazhuang, Hebei 050000, P.R. China; [2]Department of Central Laboratory, The Second Hospital of Hebei Medical University, Shijiazhuang, Hebei 050000, P.R. China; [3]Hebei Key Laboratory of Etiology Tracing and Individualized Diagnosis and Treatment for Digestive System Carcinoma, The Second Hospital of Hebei Medical University, Shijiazhuang, Hebei 050000, P.R. China

Received May 13, 2026; Accepted September 10, 2026

DOI: 10.3892/or.2026.9199

Abstract. The present study aimed to characterize the expression pattern and biological function of sphingosine-1-phosphate phosphatase 1 (SGPP1) in esophageal squamous cell carcinoma (ESCC), investigate its potential molecular regulatory mechanisms, and evaluate its clinical value as a prognostic biomarker and therapeutic target. SGPP1 expression in ESCC cell lines was assessed by reverse transcription-quantitative PCR and western blotting. Models of SGPP1 overexpression in KYSE150 cells and SGPP1 knockdown in ECA109 cells were established. 5-Ethynyl-2'-deoxyuridine, Cell Counting Kit-8, colony formation, terminal deoxynucleotidyl transferase dUTP nick-end labeling, wound healing and Transwell assays were performed to systematically analyze the effects of SGPP1 on ESCC cell proliferation, apoptosis, migration and invasion. The Cancer Genome Atlas-ESCC data were integrated with Gene Ontology and Kyoto Encyclopedia of Genes and Genomes enrichment analyses, gene set enrichment analysis and UpSet plotting to identify key downstream pathways and candidate target genes. SGPP1 protein expression was evaluated by immunohistochemistry in tumor tissues from 68 patients with ESCC, and Cox regression analysis was used to assess its association with patient prognosis. The results demonstrated that SGPP1 expression varied markedly among ESCC cell lines, with low expression in KYSE150 cells and high expression in ECA109 cells. SGPP1 overexpression significantly inhibited ESCC cell proliferation, migration and invasion, and increased apoptosis-associated DNA fragmentation, whereas SGPP1 knockdown produced the opposite effects. Mechanistically, the data suggested that SGPP1 modulates extracellular matrix remodeling and xenobiotic metabolism, potentially through negative regulation of UGT1A9 and UGT2B28 expression. Clinically, low SGPP1 expression was an independent risk factor for poor prognosis in patients with ESCC (HR=6.016, 95% CI: 3.143-11.513, P<0.001), and the overall survival was significantly longer in the high-expression group than in the low-expression group (P<0.001). In conclusion, SGPP1 functions as a tumor suppressor gene in ESCC and may inhibit tumor progression by regulating UGT1A9/UGT2B28-mediated metabolic pathways. SGPP1 may therefore serve as a prognostic biomarker and a potential therapeutic target in ESCC.

Correspondence to: Dr Xiaoying Xue or Professor Huandi Zhou, Department of Radiotherapy, The Second Hospital of Hebei Medical University, 215 Heping West Road, Xinhua, Shijiazhuang, Hebei 050000, P.R. China
E-mail: xxy0636@hebmu.edu.cn
E-mail: huandizhou@hebmu.edu.cn

[*]Contributed equally

Key words: sphingosine-1-phosphate phosphatase 1, esophageal squamous cell carcinoma, prognostic biomarker, UGT1A9, UGT2B28

Introduction

Esophageal cancer (EC) is a highly aggressive malignancy with a poor prognosis and represents a major cause of cancer-related mortality worldwide (1). Its incidence varies markedly across geographic regions, and EC is histologically classified into two major subtypes: Esophageal squamous cell carcinoma (ESCC) and esophageal adenocarcinoma (2,3). In Asia, more than 90% of EC cases are those of ESCC (4). China has a high incidence of ESCC. Based on 2022 statistics, EC is the fifth leading cause of cancer-related mortality in China and accounts for ~187,500 deaths annually (5). Despite advances in surgical resection, chemotherapy and immunotherapy, the 5-year overall survival (OS) rate among patients with ESCC remains below 30%, largely because of early lymph-node metastasis, distant invasion, and the lack of effective prognostic biomarkers and therapeutic targets (6,7). This poor outcome is also attributable to the absence of specific early symptoms during the early stages of the disease, as only ~20% of patients

are diagnosed at an early stage. However, the 5-year survival rate can reach 85% among patients diagnosed at an early stage (8). Therefore, elucidating the molecular mechanisms underlying ESCC initiation and progression and identifying novel tumor suppressors or oncogenes with clinical translational potential are essential for improving the diagnosis and treatment of ESCC (9).

Sphingosine-1-phosphate phosphatase 1 (SGPP1) is a membrane-associated phosphatase involved in sphingolipid metabolism and is known to catalyze the dephosphorylation of sphingosine-1-phosphate to sphingosine (10), which involves multiple biological processes (BPs), including cell proliferation, apoptosis, migration and invasion (11,12). Numerous studies have demonstrated that SGPP1 acts as a tumor suppressor in several malignancies, including breast cancer (BC) (13,14), gastric cancer (GC) (10) and prostate cancer (PC) (15). In BC, higher SGPP1 expression is a favorable prognostic indicator of survival outcomes in patients receiving systemic treatment, particularly those with triple-negative BC (14). In GC, positive SGPP1 expression is significantly associated with longer OS and progression-free survival and serves as an independent prognostic factor (10). In PC, SGPP1 deficiency results in smaller necrotic areas in subcutaneous xenografts following radiotherapy, a higher Ki-67-positive rate, and increased microvascular density, indicating that reduced SGPP1 expression can raise promote tumor angiogenesis and radioresistance. However, SGPP1 can exert oncogenic effects in other cancer types, such as colorectal cancer (16) and glioma (17), indicating that its function is highly tissue- and cancer-type specific. The expression pattern, biological function and underlying molecular mechanisms of SGPP1 in ESCC remain largely unknown, representing an important lacuna in molecular research on ESCC.

The present study investigated the expression and function of SGPP1 in ESCC. It assessed its tumor-suppressive role and examines the underlying molecular mechanisms. The findings provide new mechanistic insights into the role of SGPP1 in ESCC and its potential clinical applications.

Materials and methods

Cell culture and transient transfection. The ESCC cell lines TE13 and KYSE30 were kindly provided by the laboratory of Professor Gao Xianshu at Peking University First Hospital. The ECA109 and KYSE150 cell lines were purchased from Shanghai Saibai Kang Biotechnology Co., Ltd. and Zhong Qiao Xin Zhou Biotechnology Co., Ltd., respectively. ECA109 and KYSE150 cells were authenticated by short tandem repeat (STR) analysis before experimental use. The cells were cultured in RPMI-1640 medium supplemented with 10% fetal bovine serum, 100 μg/ml streptomycin, and 100 U/ml penicillin and incubated at 37˚C in a humidified incubator containing 5% CO_2. The SGPP1-overexpression plasmid and its corresponding control plasmid were obtained from General Biosystems, whereas small interfering RNA (siRNA) targeting SGPP1 (siSGPP1) and the corresponding negative control (siNC) were obtained from Guangzhou RiboBio Co., Ltd. Transient transfection was performed using Lipofectamine 3000 (Thermo Fisher Scientific, Inc.) according to the manufacturer's instructions. Briefly, 2.5 μg of nucleic acid was used for transfection; the transfection mixture was removed and fresh culture medium was replaced at 6 h post-transfection. Total RNA was harvested at 24 h post-transfection, and total protein was extracted at 48 h post-transfection for subsequent assays. The target sequence of siSGPP1 was 5'-GAACTTCCTTATCGGTATA-3'. The siNC (cat. no. siN0000001; Guangzhou RiboBio Co., Ltd.) was a commercially available non-targeting control siRNA, and its exact nucleotide sequence is proprietary and was not disclosed by the manufacturer.

RNA extraction and reverse transcription-quantitative polymerase chain reaction (RT-qPCR). Total RNA was extracted from the ESCC cells using TRIzol Universal Reagent (Tiangen Biotech Co., Ltd.) based on the manufacturer's instructions. Complementary DNA was synthesized using Oligo$(dT)_{18}$ Primer (Thermo Fisher Scientific, Inc.) with Moloney Murine Leukemia Virus (M-MLV) reverse transcriptase, 5X reaction buffer, dNTP mixture, and RNase inhibitor. The reverse transcription protocol was: 65˚C for 5 min, followed by 42˚C for 60 min, 70˚C for 5 min, and then held at 4˚C. qPCR was performed in triplicate using PowerUp™ SYBR™ Green Master Mix (Thermo Fisher Scientific, Inc.) with a CFX Connect real-time system (Bio-Rad Laboratories, Inc.). The qPCR thermocycling conditions were: initial denaturation at 95˚C for 10 min; 40 cycles of denaturation at 95˚C for 10 sec, annealing at 60˚C for 20 sec, extension at 72˚C for 15 sec; followed by melting curve analysis (95˚C for 30 sec, 25˚C for 30 sec). The primer sequences used in the present study are provided in Table SI. GAPDH was used as the endogenous control. Relative gene expression, normalized to GAPDH, was calculated using the $2^{-\Delta\Delta Cq}$ method (18), where $\Delta Ct = Ct^{\text{target gene}} - Ct^{\text{GAPDH}}$ and $\Delta\Delta Ct = \Delta Ct^{\text{experimental group}} - \Delta Ct^{\text{control group}}$.

Western blotting. The cells were lysed in RIPA buffer (Beyotime Institute of Biotechnology) supplemented with protein phosphatase inhibitor (Beijing Solarbio Science & Technology Co., Ltd.). Protein concentration was determined using the BCA method with bovine serum albumin as the standard. Equal amounts of protein (20 μg) were separated by 10% SDS-PAGE and transferred onto Immobilon-P membranes (MilliporeSigma). After blocking with 5% skim milk in Tris-buffered saline containing 0.1% Tween-20 (TBST) for 1 h at room temperature, the membranes were incubated overnight at 4˚C with primary antibodies against SGPP1 (1:200; cat. no. ab129253; Abcam), UGT1A9 (1:1,000; cat. no. YP-Ab-07897; https://www.upingbio.com/), UGT2B28 (1:1,000; cat. no. P32315; ProMab Biotechnologies, Inc.) and GAPDH (1:10,000; cat. no. 10494-1-AP; Proteintech Group, Inc.). The membranes were then washed three times with TBST for 10 min per wash and incubated with the appropriate secondary antibodies [HRP-conjugated Goat Anti-Rabbit IgG (H+L); 1:8,000; cat. no. SA00001-2; Proteintech Group, Inc.] for 1 h at room temperature. Protein bands were visualized using an enhanced chemiluminescence substrate kit (Biosharp Life Sciences) and an ECL detection system (Bio-Rad Laboratories, Inc.). Protein levels were normalized exclusively to the corresponding loading control on the same membrane. GAPDH optical-density values were quantified

in each independent western blot experiment to evaluate the stability of GAPDH as a reference gene under fluctuating SGPP1 expression (Table SII).

Colony formation assay. Cell proliferation was evaluated using a colony formation assay. The cells were counted, seeded into 6-well plates at a density of 50 cells per well, and incubated at 37˚C incubator for 14 days without disturbance. Following fixation with methanol and staining with 0.1% crystal violet, colonies containing at least 50 cells were counted under a light microscope.

Cell Counting Kit-8 (CCK-8) assay. Cell proliferation was evaluated using the CCK-8 assay (MedChemExpress). A total of $3x10^3$ cells per well were seeded into 96-well plates in triplicate, and 10 μl of CCK-8 solution was added to each well at seven designated time points. Following incubation for 1.5 h incubation at 37˚C, absorbance at 450 nm was measured using an Infinite M200 Pro NanoQuant instrument (Tecan Group, Ltd.). Cell viability was calculated using the following formula: OD of the experimental group/OD of the control group x100%.

5-Ethynyl-2'-deoxyuridine (EdU) incorporation assay. EdU incorporation was assessed using a Cell-Light EdU DNA Cell Proliferation Kit (Guangzhou RiboBio Co., Ltd.) based on the manufacturer's instructions. Briefly, the treated cells were seeded into 24-well plates at a density of $2x10^4$ cells per well and cultured for 48 h. The cells were then stained for EdU incorporation at 37˚C for 2 h based on the manufacturer's protocol. Fluorescence images were acquired using an inverted fluorescence microscope, and the percentage of EdU-positive cells was quantified as an indicator of cell proliferation.

Terminal deoxynucleotidyl transferase dUTP nick-end labeling (TUNEL) assay. The treated cells were seeded into 48-well plates at a density of $1x10^4$ cells per well and incubated for 24 h. Apoptosis was assessed using a TUNEL apoptosis detection kit (Nanjing KeyGen Biotech Co., Ltd.) based on the manufacturer's instructions. The nuclei were counterstained with DAPI (0.001 mg/ml, blue), whereas apoptotic cells were identified based on green fluorescence. Images were acquired using an inverted fluorescence microscope.

Transwell migration and invasion assay. Transwell chambers with 8-μm pores (Corning, Inc.) were utilized to perform migration and invasion assays. Before the assays, the cells were serum-starved in FBS-free RPMI-1640 medium for 24 h. For the invasion assays, the upper chambers were precoated with Matrigel (BD Biosciences) and incubated at 37˚C for 6 h, whereas this step was omitted for migration assays. After the Matrigel had solidified, $2x10^4$ cells for the migration assays or $4x10^4$ cells for the invasion assays were suspended in 150 μl of serum-free medium and seeded into the upper chambers. The lower chambers were filled with 600 μl of medium containing 10% FBS as a chemoattractant. After 48 h, the cells remaining on the upper surface of the membrane were removed using a cotton swab, and the migratory or invasive cells were stained with crystal violet (Beijing Solarbio Science & Technology Co., Ltd.). The cells were counted in three randomly selected fields per well, and the mean number of cells per field was calculated.

Monolayer cell migration scratch assay. Cells were seeded in 6-well plates and cultured to 80-90% confluence. A uniform scratch wound was generated across the cell monolayer using a sterile pipette tip. After the cells were washed with PBS, the culture medium was replaced with serum-free medium. Images of three randomly selected fields per well were acquired at 0, 12 and 24 h. Wound closure was quantified using ImageJ software (v2.9.0; National Institutes of Health).

Bioinformatics analysis of The Cancer Genome Atlas (TCGA)-ESCC RNA-sequencing (RNA-seq) data. Based on data obtained from TCGA database (https://portal.gdc.cancer.gov/), the RNA-seq data for esophageal carcinoma (ESCA) and the corresponding clinicopathological information were acquired. ESCC samples were selected based on histological type. Only samples classified as squamous cell carcinoma in the clinical information were retained, whereas samples without corresponding clinical information were excluded. A total of 82 ESCC samples were ultimately included in differentially expressed gene (DEG) analysis, SGPP1 correlation analysis, and the Pearson correlation analyses. All subsequent bioinformatics analyses and statistical evaluations were performed using R software (version 4.2.1; https://www.r-project.org/). The samples were stratified into subgroups using the median SGPP1 expression level as the cutoff value. Differential expression analysis was subsequently performed using DESeq2 version 1.36.0 with the filtering criteria of $|\log_2$ fold change (FC)$|>1$, $P<0.05$ and adjusted $P<0.05$. This analysis identified 271 upregulated DEGs (up-DEGs) and 435 downregulated DEGs (down-DEGs). In addition, gene correlation analysis was performed using Pearson correlation analysis in R version 4.2.1, and P values were adjusted using the Benjamini-Hochberg method. The threshold for the correlation coefficient was set at $|Cor|>0.3$, resulting in the identification of 516 genes positively correlated with SGPP1 expression and 569 genes negatively correlated with SGPP1 expression.

For functional annotation of the candidate genes, the intersection between up-DEGs and SGPP1-positively correlated genes and the intersection between down-DEGs and SGPP1-negatively correlated genes, were separately subjected to Gene Ontology (GO) functional enrichment analysis and Kyoto Encyclopedia of Genes and Genomes (KEGG) pathway enrichment analysis. In parallel, gene set enrichment analysis (GSEA) based on the KEGG database was performed for the ESCC dataset. Before GO/KEGG enrichment analysis, all input gene lists underwent ID conversion, followed by enrichment analysis using clusterProfiler version 4.4.4 (https://yulab-smu.top/clusterProfiler-book/). GOplot version 1.0.2 (http://cran.r-project.org/web/packages/GOplot) was utilized to calculate term z-scores from gene-level metrics to indicate the overall trends in gene upregulation or downregulation for each enriched entry, whereas ggplot2 version 3.4.4 was employed to visualize all GO and KEGG enrichment results. GSEA was performed using clusterProfiler version 4.4.4. Genes were annotated using org.Hs.eg.db, and the analysis employed the KEGG gene set c2.cp.kegg.v7.5.1.symbols.gmt imported through msigdbr. The results were visualized using ggplot2 version 3.4.4. GSEA was performed using clusterProfiler version 4.4.4 in R version 4.2.1. Genes were ranked according to the log2FC between the SGPP1-high and

SGPP1-low groups. Gene identifiers were annotated using org.Hs.eg.db, and the KEGG gene set c2.cp.kegg.v7.5.1.symbols.gmt, obtained through msigdbr, was used as the reference gene-set collection. GSEA was performed with 1,000 permutations, with the minimum and maximum gene-set sizes set to 15 and 500, respectively. Pathways with a nominal P<0.05, FDR q-value <0.25, and |NES|>1.5 were considered significant. GSEA results were visualized using ggplot2 version 3.4.4 (https://ggplot2.tidyverse.org/).

Core signaling pathways were ultimately identified by intersecting the pathways enriched in the KEGG analysis of the intersecting gene sets with those identified through GSEA-KEGG analysis. This approach facilitated the identification of molecular pathways potentially underlying the effects of SGPP1 on ESCC cell behavior.

Immunohistochemical (IHC) validation of SGPP1 protein expression. After baking at 65˚C for 4 h, ESCC tissue sections were deparaffinized in xylene (3x10 min) and rehydrated through a graded ethanol series (100, 95, 85, and 75%; 8 min per step). Antigen retrieval was performed out in 1X EDTA buffer in a 95˚C water bath for 1 h, and endogenous peroxidase activity was blocked using 3% H_2O_2 for 30 min at room temperature. The sections were incubated overnight at 4˚C with an anti-SGPP1 primary antibody (1:50), followed by incubation with an HRP-conjugated goat anti-mouse/rabbit IgG polymer detection system (ready-to-use; cat. no. PV-9000; OriGene Technologies, Inc.) for 1 h at 37˚C. DAB development was monitored microscopically and terminated after 1 min. The slides were counterstained with hematoxylin, dehydrated through a graded ethanol series, cleared, and cover-slipped using a neutral mounting medium. Staining intensity was quantified using ImageJ. IHC staining was semi-quantitatively scored based on staining intensity and the percentage of positive cells. Staining intensity was classified as absent, pale yellow, brownish yellow, or dark brown and assigned scores of 0, 1, 2, and 3, respectively. The percentage of positively stained cells was scored as follows: 0%=0, 5-25%=1, 26-50%=2, 51-75%=3, and >75%=4. The final score was calculated as the sum of the staining intensity score and the percentage score. A summed score <6 was employed to define the low-expression group, whereas a score ≥6 was utilized to define the high-expression group. For each section, three randomly selected fields were examined at x400 magnification; staining intensity and the percentage of positive cells were scored in each field, and the mean score was calculated. Two pathologists independently evaluated the IHC staining in a double-blind manner.

Patients and samples. This single-center, retrospective, tissue-based cohort study included patients with primary ESCC identified through the pathology archive and clinical follow-up system of the Second Hospital of Hebei Medical University between January 2010 and December 2024. The inclusion criteria were as follows: i) pathologically confirmed primary ESCC; ii) a Karnofsky Performance Status (KPS) score>70; iii) receipt of radical radiotherapy at a total dose (DT) ≥50 Gy; iv) availability of sufficient formalin-fixed, paraffin-embedded tumor tissue for SGPP1 IHC; v) complete clinicopathological, treatment, and OS follow-up data; and vi) ethical approval and informed consent. The exclusion criteria were as follows: i) non-squamous or mixed histology; ii) a history of another malignancy; iii) insufficient tissue or non-evaluable IHC staining; and iv) missing key clinical variables or follow-up information. A total of 68 patients were included in the study, including 39 males and 29 females, with a median age of 69 years (range, 24-87 years). A detailed patient enrollment flowchart has been provided (Fig. S1). Tissue specimens were fixed in 4% formalin at room temperature for 24-48 h and embedded in paraffin. Samples were obtained with patient consent under approval from the Ethics Committee of The Second Hospital of Hebei Medical University (approval no. 2024-R393; Shijiazhuang, China). OS was defined as the interval from the date of pathological diagnosis to death or the last confirmed follow-up. Patients who remained alive at the follow-up cutoff date were censored at their last confirmed follow-up date.

Statistical analysis. All experiments were conducted at least three times. Data are presented as the mean ± SD. Statistical analyses were performed using GraphPad Prism 8.0 software (Dotmatics). Paired or unpaired Student's t-tests and one-way or two-way analyses of variance (ANOVA) followed by Bonferroni's post hoc test were applied as appropriate. Survival curves were generated using the Kaplan-Meier method and compared using a two-sided log-rank test. Cox proportional hazards regression models were used for univariate and multivariate analyses. The proportional hazards assumption was assessed and was satisfied. P<0.05 was considered to indicate a statistically significant difference.

Results

Verification of SGPP1 knockdown and overexpression efficiency. Western blotting and RT-qPCR analyses revealed distinct SGPP1 expression patterns among the four EC cell lines (TE13, KYSE150, ECA109 and KYSE30). SGPP1 mRNA expression was significantly higher in ECA109 and KYSE30 cells than in TE13 and KYSE150 cells (Fig. 1A). At the protein level, SGPP1 expression was relatively high in ECA109 and KYSE30 cells and comparatively low in TE13 and KYSE150 cells, with KYSE150 cells exhibiting the lowest protein expression among the four cell lines (Fig. 1B). Based on these expression profiles, KYSE150 cells, which exhibited relatively low endogenous SGPP1 expression, were utilized to establish a stable SGPP1-overexpression model (OE), whereas ECA109 cells, which exhibited relatively high endogenous SGPP1 expression, were used for transient SGPP1 knockdown with siRNA (siSGPP1). RT-qPCR analysis confirmed that SGPP1 mRNA levels were significantly increased in the OE group (P<0.0001 vs. Vector/Blank) and significantly decreased in siSGPP1 cells (P=0.001, vs. Blank; P=0.0023 vs. NC). No significant differences were observed between the corresponding control groups (Fig. 1C and D). Western blotting and densitometric analyses further confirmed significant upregulation of SGPP1 protein in the OE group compared with the Blank (P=0.0345) and Vector (P=0.0417) groups (Fig. 1E and F), as well as significant downregulation in the siSGPP1 group compared with the NC group (P=0.0349; Fig. 1G and H). These results confirmed the successful establishment of the SGPP1-OE model in KYSE150 cells and efficient SGPP1 knockdown in ECA109 cells.

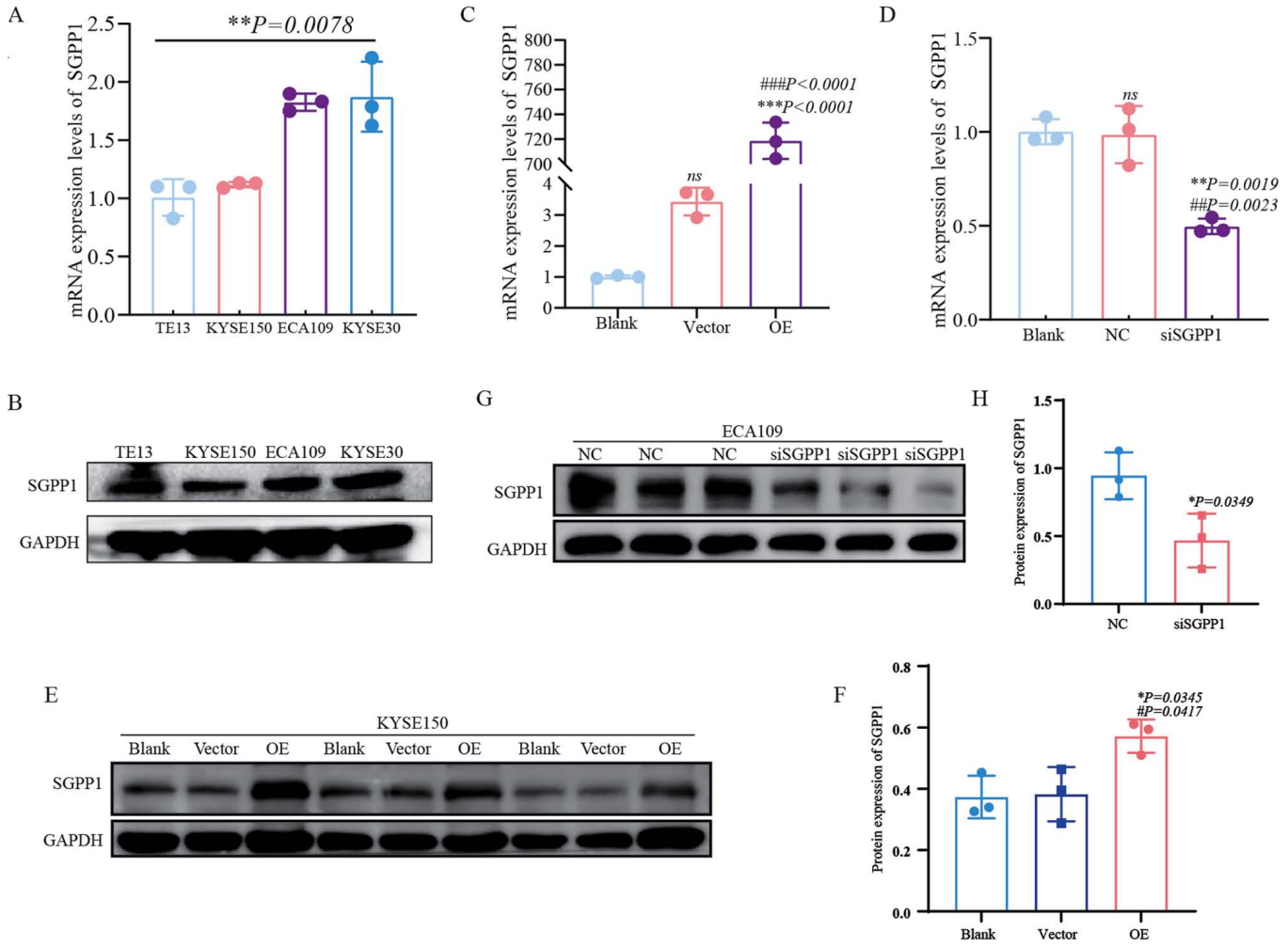

Figure 1. Verification of SGPP1 knockdown and overexpression efficiency. (A and B) SGPP1 expression in four esophageal cancer cell lines (TE13, KYSE150, ECA109 and KYSE30) was assessed by (A) RT-qPCR and (B) western blotting. (C and D) RT-qPCR validation of (C) SGPP1 overexpression in KYSE150 cells (Blank, Vector, and OE groups) and (D) SGPP1 knockdown in ECA109 cells (Blank, NC, and siSGPP1 groups). (E and F) The results of (E) western blots and (F) densitometric quantification of SGPP1 protein expression in KYSE150 cells after SGPP1 overexpression. (G and H) The results of (G) western blots and (H) densitometric quantification of SGPP1 protein expression in ECA109 cells after SGPP1 knockdown. SGPP1, sphingosine-1-phosphate phosphatase 1; RT-qPCR, reverse transcription-quantitative PCR; si-, small interfering; OE, overexpression; NC, negative control; ns, not significant.

Effects of SGPP1 on the proliferation and apoptosis of EC cells. EdU immunofluorescence staining was performed to evaluate ESCC cell proliferation. In KYSE150 cells, the percentage of EdU-positive cells was significantly lower in the SGPP1-OE group than in the Vector group (Fig. 2A, P=0.005). By contrast, SGPP1 silencing in ECA109 cells significantly increased the percentage of EdU-positive cells compared with the NC group (Fig. 2B, P=0.0079). These results indicated that SGPP1 inhibited ESCC cell proliferation. Colony formation assays were performed to evaluate long-term proliferative capacity of ESCC cells. In KYSE150 cells, the OE group formed significantly fewer colonies than the Vector group (Fig. 2C, P=0.0067). In ECA109 cells, SGPP1 knockdown significantly increased colony formation compared with the NC group (Fig. 2D, P=0.0473). These findings further demonstrated that SGPP1 suppressed the long-term proliferative capacity of ESCC cells. CCK-8 assays were performed to monitor cell viability over time. In KYSE150 cells, SGPP1 overexpression reduced optical density values throughout the 7-day culture period. Cell viability was slightly lower in the OE group than in the Vector group on days 2 and 3, although these differences were not statistically significant. From days 4 to 7, cell viability remained significantly lower in the OE group (Fig. 2E, P<0.001). In ECA109 cells, cell viability was significantly higher in the siSGPP1 group than in the NC group from days 2 to 7 (Fig. 2F, P<0.001). Collectively, these findings indicated that SGPP1 suppresses ESCC cell proliferation over time.

TUNEL staining was performed to assess apoptosis in ESCC cells. In KYSE150 cells, the percentage of TUNEL-positive apoptotic cells was significantly higher in the OE group than in the Vector group (Fig. 2G, P=0.0003). In ECA109 cells, the apoptotic rate was significantly lower in the siSGPP1 group than in the NC group (Fig. 2H, P=0.0012). These results indicated that SGPP1 increases apoptosis-associated DNA fragmentation in ESCC cells.

Effects of SGPP1 on the migration and invasion of EC cells. The effects of SGPP1 on ESCC cell migration and invasion were evaluated in KYSE150 and ECA109 cells

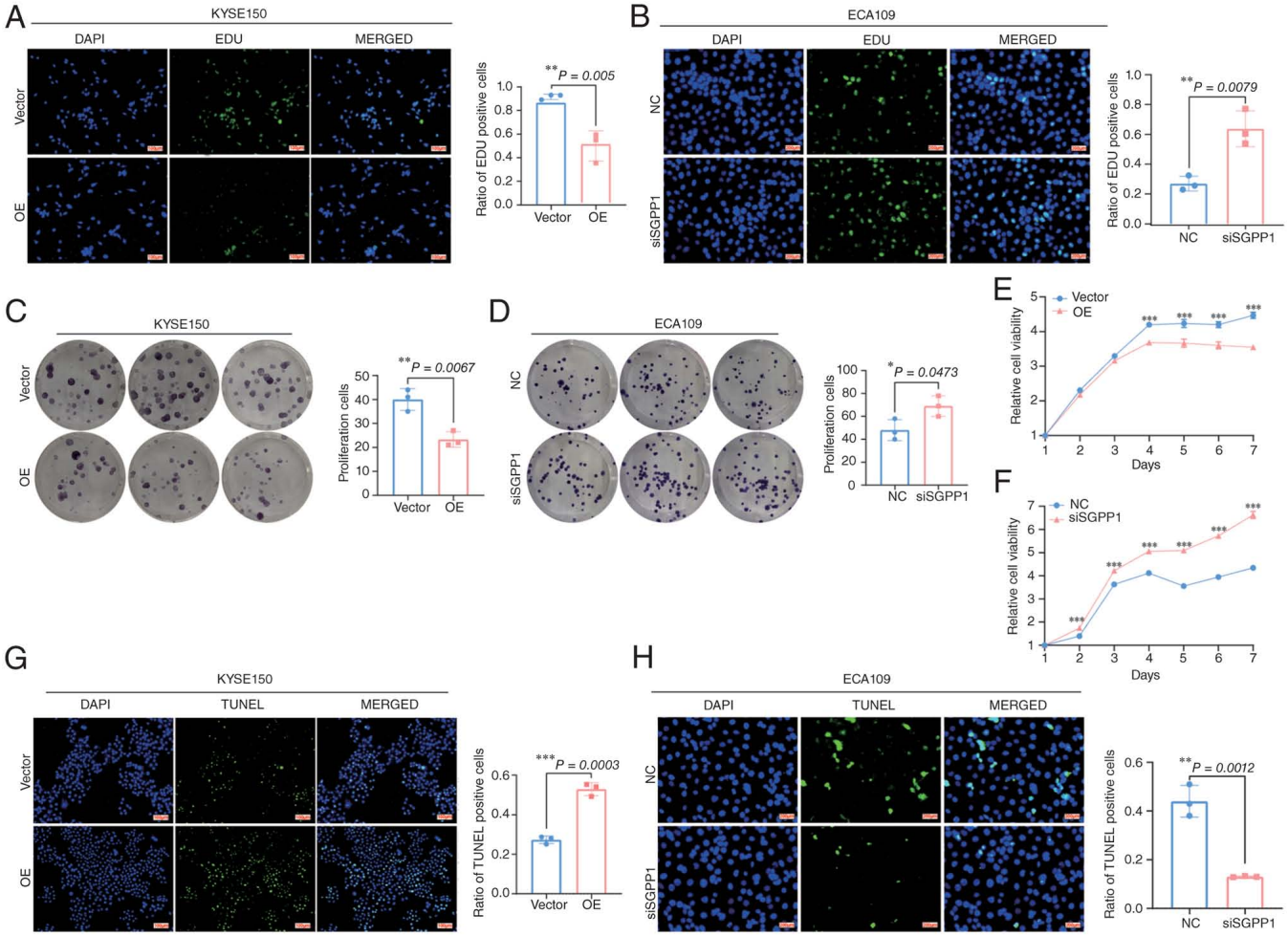

Figure 2. Effects of SGPP1 on the proliferation and apoptosis of esophageal cancer cells. (A and B) EdU assays in (A) KYSE150 cells and (B) ECA109 cells. (C and D) Colony formation assays in (C) KYSE150 cells and (D) ECA109 cells. (E and F) Cell Counting Kit-8 assays in (E) KYSE150 cells and (F) ECA109 cells. ***P<0.001. (G and H) TUNEL assays in (G) KYSE150 cells and (H) ECA109 cells. SGPP1, sphingosine-1-phosphate phosphatase 1; EdU, 5-Ethynyl-2'-deoxyuridine; TUNEL, terminal deoxynucleotidyl transferase dUTP nick-end labeling; si-, small interfering; OE, overexpression; NC, negative control; ns, not significant.

using wound-healing and Transwell assays. In KYSE150 cells, the migration rate in the OE group was significantly lower than that in the Vector group at 12 h (P=0.0308) and 24 h (P=0.0455) in the wound-healing assay, indicating that SGPP1 overexpression inhibited cell migration (Fig. 3A). By contrast, the wound-closure rate was significantly higher in the siSGPP1 group than in the NC group at 12 and 24 h (P<0.001), indicating that SGPP1 knockdown raised ECA109 cell migration (Fig. 3B). Under the experimental conditions, KYSE150 cells exhibited lower basal migratory activity than ECA109 cells, resulting in a lower wound-closure rate over the 24 h observation period. Therefore, the apparent differences in migration rates between KYSE150 and ECA109 cells primarily reflected their intrinsic biological characteristics. Transwell assays further showed that the numbers of migratory and invasive KYSE150 cells were significantly lower in the OE group than that in the Vector group (Fig. 3C; migration, P=0.0009; invasion, P=0.0060). By contrast, the numbers of migratory and invasive ECA109 cells were significantly higher in the siSGPP1 group than in the NC group (Fig. 3D; migration, P=0.0026; invasion, P=0.0004). These results indicated that SGPP1 can improve the migration and invasion abilities of ECA109 cells. These findings therefore indicated that SGPP1 negatively regulates the migratory and invasive properties of ESCC cells.

Molecular regulatory mechanisms of SGPP1 in EC. Using the ESCC subset of the TCGA-ESCA cohort (n=82), a volcano plot was generated to identify significantly upregulated (red), downregulated (blue) and non-significant (black) DEGs based on the thresholds $|log_2FC|>1$, P<0.05 and adjusted P<0.05 (Fig. 4A). Integration of the differential expression results with the correlation analysis identified the core gene sets. The intersection of up-DEGs and positively correlated genes (Cor-positive) comprised 102 genes (Fig. 4B), whereas the intersection of down-DEGs and negatively correlated genes (Cor-negative) comprised 122 genes (Fig. 4C). These gene sets were separately subjected to GO functional enrichment analysis. For the upregulated and downregulated gene sets, the top five molecular function (MF) and BP terms were displayed; cellular component terms were not presented because no meaningful enrichment was identified. The upregulated intersecting genes were significantly enriched in extracellular matrix (ECM)-related BPs, including ECM organization, extracellular structure organization, and external encapsulating structure organization. Enriched MFs included

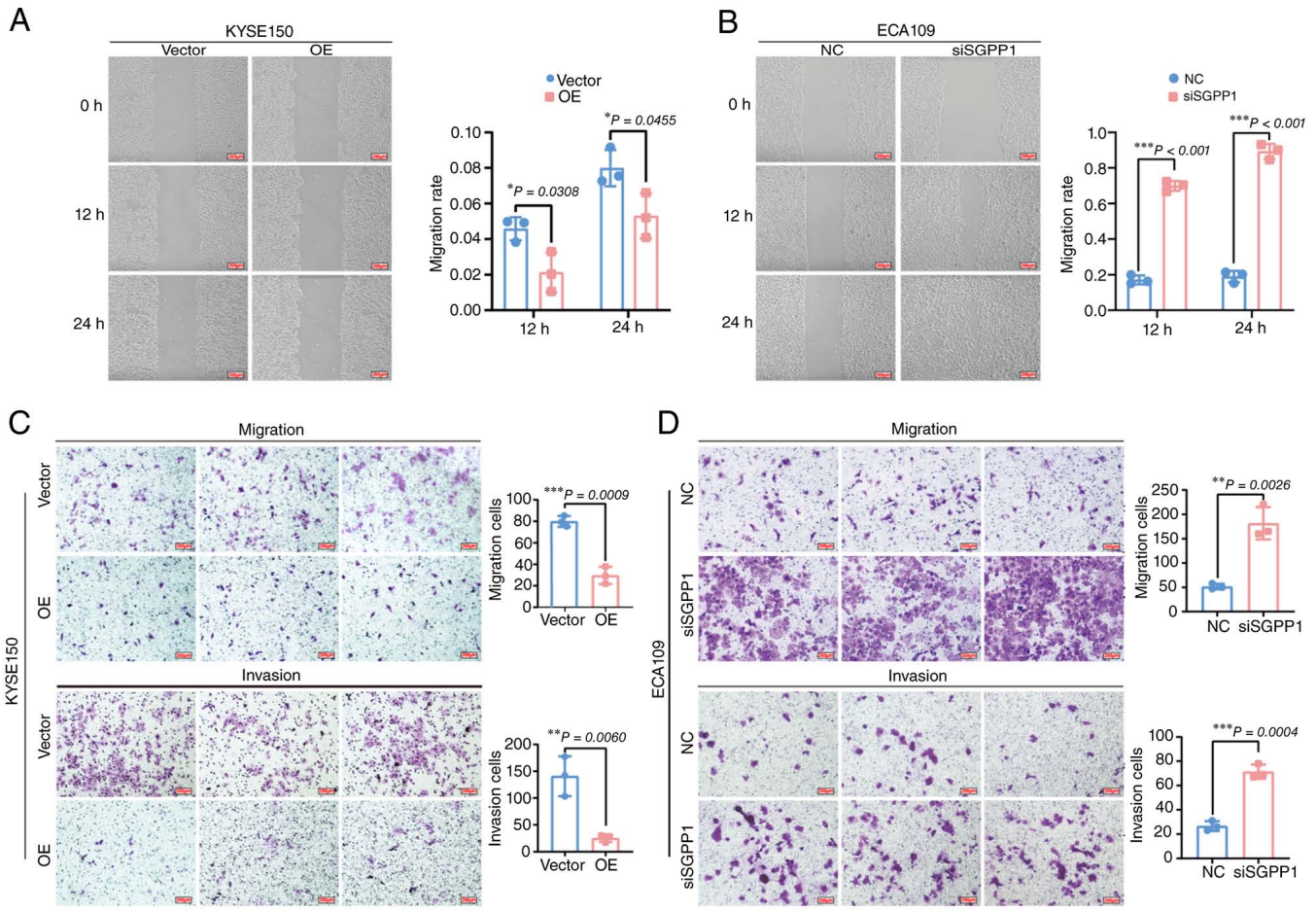

Figure 3. Effects of SGPP1 on the migration and invasion of esophageal cancer cells. (A) Wound-healing images and quantitative analysis of KYSE150 cells in the Vector and OE groups at 0, 12, and 24 h. (B) Wound-healing images and quantitative analysis of ECA109 cells in the NC and siSGPP1 groups at 0, 12, and 24 h. (C) Upper panel: Transwell migration images and quantitative analysis of KYSE150 cells in the Vector and OE groups. Lower panel: Transwell invasion images and quantitative analysis of KYSE150 cells in the Vector and OE groups. (D) Upper panel: Transwell migration assay images and quantitative analysis of ECA109 cells in the NC and siSGPP1 groups. Lower panel: Transwell invasion images and quantitative analysis of ECA109 cells in the NC and siSGPP1 groups. SGPP1, sphingosine-1-phosphate phosphatase 1; OE, overexpression; si-, small interfering; NC, negative control.

signaling receptor activator activity, metallo-endopeptidase activity, heparin binding, and cytokine activity, whereas the enriched BPs also included positive regulation of calcium ion transport into the cytosol. These findings indicated that higher SGPP1 expression is associated with ECM remodeling and cytokine-mediated signaling (Fig. 4D). The downregulated intersecting genes were predominantly enriched in xenobiotic metabolism and stimulus-response processes, including xenobiotic metabolic process, cellular response to xenobiotic stimulus, and response to xenobiotic stimulus. Enriched MFs included iron ion binding, arachidonic acid monooxygenase activity, arachidonic acid epoxygenase activity, neuropeptide receptor binding, and retinoic acid 4-hydroxylase activity. Retinoid and olefinic compound metabolic process were also enriched. These findings indicated that higher SGPP1 expression is associated with the suppression of pathways involved in xenobiotic detoxification and retinoid and arachidonic acid metabolism (Fig. 4E).

KEGG enrichment analysis was performed separately for the 102 upregulated and 122 downregulated intersecting genes (Fig. 4F and G). GSEA was performed to validate the pathways identified through KEGG enrichment analysis (Fig. 4H and I). In the upregulated direction, four significant DEG-KEGG pathways were identified, three of which overlapped with the GSEA-KEGG results: Focal adhesion, ECM-receptor interaction, and cytokine-cytokine receptor interaction (Fig. 4H). In the downregulated direction, five significant DEG-KEGG pathways were identified, four of which overlapped with the GSEA-KEGG results: Drug metabolism cytochrome P450, metabolism of xenobiotics by cytochrome P450, drug metabolism-other enzymes and retinol metabolism (Fig. 4I).

A gene-level intersection analysis was performed using the KEGG enrichment results for the downregulated core DEGs and the transcriptomic signatures obtained through GSEA, and the results were visualized using an UpSet plot (Fig. 4J) to identify the core signaling network regulated by SGPP1. The UpSet plot summarized the overlap between the DEG-KEGG and GSEA-KEGG pathways and facilitated the identification of genes consistently enriched across all downregulated pathways. UGT1A9 and UGT2B28 were the only genes present across all overlapping downregulated pathways and were therefore prioritized for correlation analysis and mRNA- and protein-level validation. Pearson correlation analysis of TCGA-ESCC transcriptomic data (n=82) revealed modest inverse correlations between SGPP1 and UGT1A9 (Pearson R=-0.366, R^2=0.134, P<0.001) and between SGPP1 and UGT2B28 (Pearson R=-0.405,

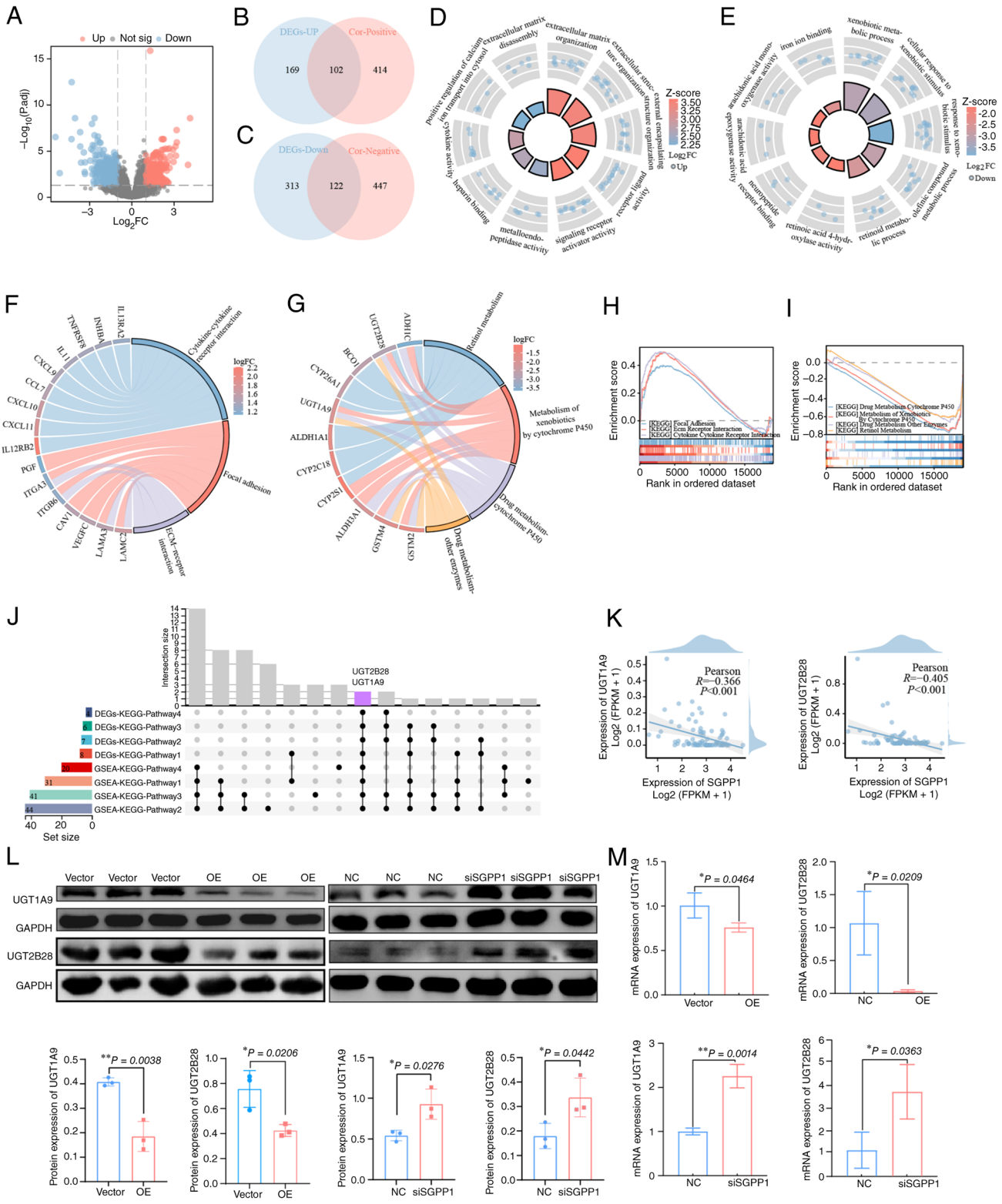

Figure 4. Molecular regulatory mechanisms of SGPP1 in esophageal cancer. (A) Volcano plot of DEGs identified according to SGPP1 expression in TCGA-ESCC dataset; red, blue, and gray dots represent significantly upregulated, downregulated and non-significant genes, respectively. (B) Venn diagram showing the intersection of upregulated DEGs and genes positively correlated with SGPP1 in the TCGA-ESCC dataset. (C) Venn diagram showing the intersection of downregulated DEGs and genes negatively correlated with SGPP1 in the TCGA-ESCC dataset. (D and E) Gene Ontology enrichment analyses of the (D) 102 upregulated intersecting genes and (E) 122 downregulated intersecting genes. (F and G) KEGG pathway enrichment analyses of the (F) 102 upregulated intersecting genes and (G) 122 downregulated intersecting genes. (H and I) Intersections of GSEA-KEGG results with the (H) up-DEGs-KEGG and (I) down-DEGs-KEGG results. (J) UpSet plot showing genes shared among 4 down-DEGs-KEGG pathways and 4 GSEA-KEGG pathways. (K) Correlations of SGPP1 expression with UGT1A9 and UGT2B28 expression in the TCGA-ESCC dataset. (L) Western blotting and quantitative analyses of UGT1A9 and UGT2B28 protein expression in KYSE150 cells after SGPP1 overexpression (Vector vs. OE) and in ECA109 cells after SGPP1 knockdown (NC vs. siSGPP1). (M) Reverse transcription-quantitative PCR analysis of UGT1A9 and UGT2B28 mRNA expression in KYSE150 cells after SGPP1 overexpression and in ECA109 cells after SGPP1 knockdown. SGPP1, sphingosine-1-phosphate phosphatase 1; DEGs, differentially expressed genes; TCGA, The Cancer Genome Atlas; ESCC, esophageal squamous cell carcinoma; KEGG, Kyoto Encyclopedia of Genes and Genomes; GSEA, gene set enrichment analysis; OE, overexpression; si-, small interfering; NC, negative control; up-DEGs, upregulated DEGs; down-DEGs, downregulated DEGs.

Table I. Association of SGPP1 expression with clinicopathological characteristics and univariate and multivariate Cox regression analyses of overall survival in 68 patients with esophageal squamous cell carcinoma.

		Univariate analysis		Multivariate analysis	
Characteristics	Total (n=68)	HR (95% CI)	P-value	HR (95% CI)	P-value
Age, years					
≥60	51	Reference			
<60	17	0.897 (0.488-1.649)	0.727		
Sex	68				
Male	39	Reference			
Female	29	1.362 (0.799-2.322)	0.256		
Lesion location	68				
Middle + lower thoracic segments	41	Reference			
Cervical + upper thoracic segments	27	0.691 (0.399-1.196)	0.187		
Lesion length, cm	68				
<5	30	Reference			
≥5	38	1.207 (0.704-2.069)	0.495		
Clinical stage	68				
I + II	43	Reference			
III + IV	25	0.671 (0.382-1.178)	0.164		
Lymphatic invasion	68				
No	20	Reference			
Yes	48	1.198 (0.670-2.144)	0.542		
Concurrent chemoradiotherapy	68				
No	37	Reference		Reference	
Yes	31	0.482 (0.277-0.837)	0.010	0.319 (0.180-0.567)	<0.001
Expression of SGPP1	68				
High (≥6)	31	Reference		Reference	
Low (<6)	37	4.297 (2.322-7.952)	<0.001	6.016 (3.143-11.513)	<0.001

SGPP1, sphingosine-1-phosphate phosphatase 1; HR, hazard ratio; CI, confidence interval.

R^2=0.164, P<0.001) (Fig. 4K). Western blotting and densitometric quantification analyses (Fig. 4L) were performed to assess the relationship between SGPP1 and UGT1A9/UGT2B28 in ESCC cell lines. In KYSE150 cells, SGPP1 overexpression significantly decreased UGT1A9 (P=0.0038) and UGT2B28 (P=0.0206) protein levels relative to those in the Vector group. In ECA109 cells, SGPP1 knockdown significantly increased the protein levels of UGT1A9 (P=0.0276) and UGT2B28 (P=0.0442) compared with those in the NC group. RT-qPCR analysis (Fig. 4M) consistently demonstrated that SGPP1 overexpression significantly reduced UGT1A9 and UGT2B28 mRNA expression in KYSE150 cells (UGT1A9, P=0.0464; UGT2B28, P=0.0209), whereas SGPP1 knockdown significantly increased their mRNA expression in ECA109 cells (UGT1A9, P=0.0014; UGT2B28, P=0.0363). These gain- and loss-of-function data demonstrated that SGPP1 negatively regulates UGT1A9 and UGT2B28 expression at the mRNA and protein levels, consistent with the inverse correlations observed in the TCGA-ESCC cohort. The TCGA-ESCC correlation analysis and *in vitro* validation support UGT1A9 and UGT2B28 as candidate downstream mediators of SGPP1 in ESCC.

SGPP1 association with survival and prognosis in patients with EC. The follow-up cutoff date for this cohort was December 31, 2025. All 68 patients completed follow-up, corresponding to a follow-up rate of 100%. The follow-up duration ranged from 2 to 119 months, with a median duration of 19.5 months. IHC was performed to evaluate SGPP1 protein expression in tumor tissues obtained from 68 patients with ESCC. SGPP1 protein expression varied markedly among the tumor samples, indicating a heterogeneous expression pattern within the cohort. The general clinicopathological characteristics of the patients and the results of the univariate and multivariate Cox regression analyses are listed in Table I.

Among the 68 patients with ESCC, 51 were aged ≥60 years and 17 were aged <60 years; 39 were male and 29 were female. Lesions were located in the middle or lower thoracic segments in 41 patients and in the cervical or upper thoracic segments in 27 patients. Lesion length was <5 cm in 30 patients and ≥5 cm in 38 patients. In total, 43 patients had clinical stage I or II disease, whereas 25 had stage III or IV disease. Lymphatic invasion was present in 48 patients and absent in 20 patients. A total of 31 patients received concurrent chemoradiotherapy,

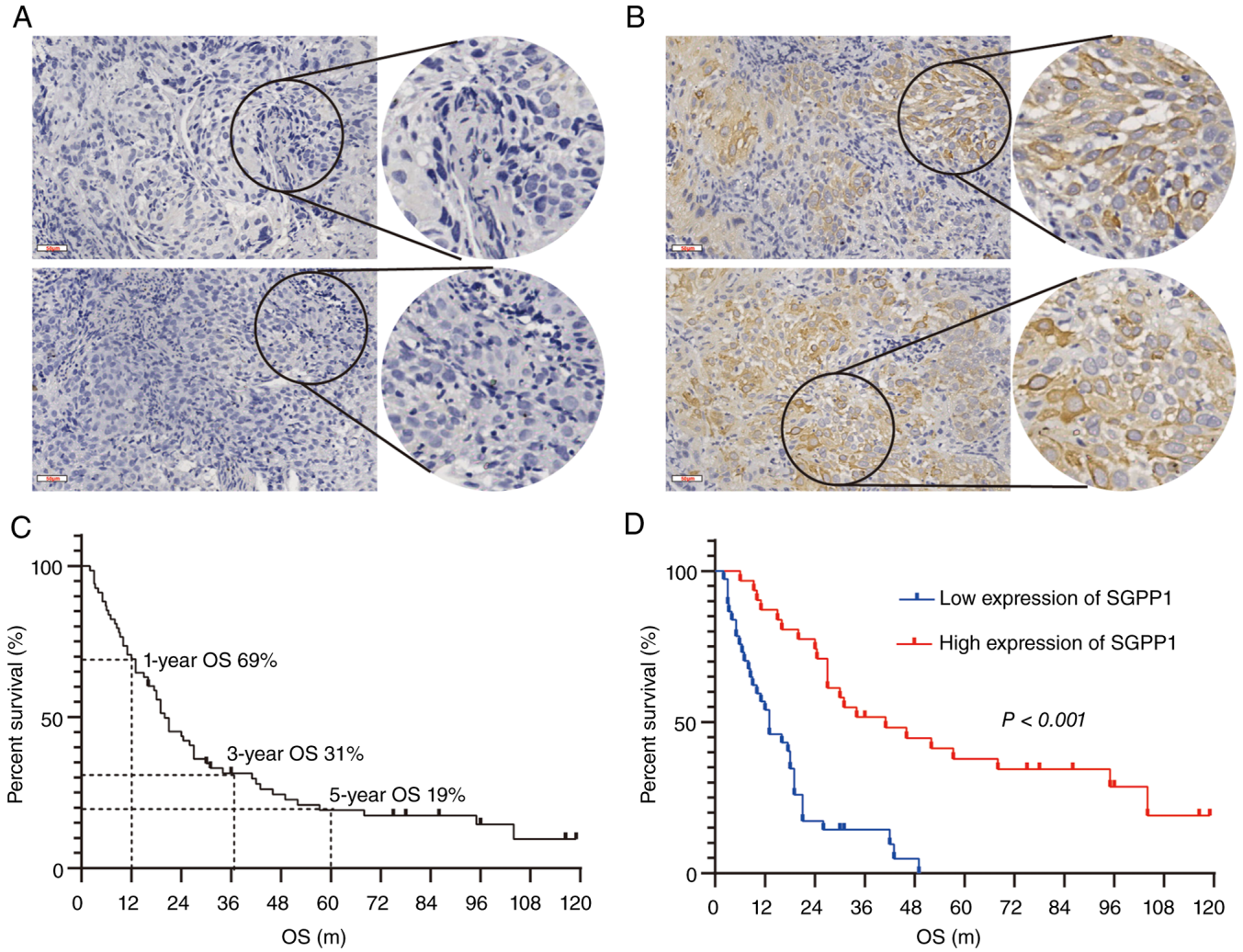

Figure 5. Association of SGPP1 expression with survival and prognosis in patients with esophageal cancer. (A and B) Representative immunohistochemical staining of ESCC tissues with (A) low SGPP1 expression and (B) high SGPP1 expression; the right panels show enlarged views of the indicated areas. (C) OS curve for all 68 patients with ESCC, showing the 1-,3-, and 5-year OS rates. (D) OS curves for the low-SGPP1-expression (blue) and high-SGPP1-expression (red) groups. SGPP1, sphingosine-1-phosphate phosphatase 1; ESCC, esophageal squamous cell carcinoma; OS, overall survival.

whereas 37 received radiotherapy alone. Representative IHC images demonstrated the heterogeneous SGPP1 expression pattern in clinical ESCC specimens. A representative tumor with low or negative SGPP1 expression, characterized by weak or absent cytoplasmic immunoreactivity is shown in Fig. 5A, whereas a representative tumor with high or positive SGPP1 expression, characterized by strong and distinct cytoplasmic staining, is demonstrated in Fig. 5B. The 1-, 3- and 5-year OS rates among the 68 patients in this group were 69, 31 and 19%, respectively (Fig. 5C). Based on the IHC scores, 31 tumors exhibited high SGPP1 expression (score ≥6), whereas 37 tumors exhibited had low SGPP1 expression (score <6). Univariate Cox regression analysis showed that concurrent chemoradiotherapy (HR=0.482, 95% CI: 0.277-0.837, P=0.010) and SGPP1 expression level (HR=4.297, 95% CI: 2.322-7.952, P<0.001) were significantly associated with OS. Age, sex, lesion location, lesion length, clinical stage and lymphatic invasion were not significantly associated with prognosis (all P>0.05). Variables that were significant in the univariate analysis were entered into the multivariate Cox regression model. Concurrent chemoradiotherapy was independently associated with a favorable prognosis (HR=0.319, 95% CI: 0.180-0.567, P<0.001), whereas low SGPP1 expression was an independent risk factor for the poor prognosis (HR=6.016, 95% CI: 3.143-11.513, P<0.001) (Table I). Patients in the high-SGPP1 expression group had significantly longer OS than those in the low expression group (P<0.001) (Fig. 5D).

Discussion

The present study systematically investigated the biological functions and molecular mechanisms of SGPP1 in ESCC and identified SGPP1 as a tumor suppressor whose low expression is associated with poor prognosis. The findings demonstrated that SGPP1 inhibits ESCC cell proliferation, viability, migration and invasion while promoting apoptosis. Mechanistically, SGPP1 can exert its tumor-suppressive effects by negatively regulating UGT1A9 and UGT2B28 expression and modulating ECM remodeling and xenobiotic metabolic pathways. In addition, SGPP1 expression was identified as an independent prognostic factor in patients with ESCC, supporting its potential utility as a prognostic biomarker and therapeutic target.

These findings are consistent with the tumor-suppressive role of SGPP1 reported in several solid tumors, including BC (13), GC (10) and PC (15). In the present study, it was demonstrated that SGPP1 expression was heterogeneous among the ESCC cell lines examined, with relatively low endogenous expression in KYSE150 cells and relatively high expression in ECA109 cells. Gain- and loss-of-function experiments using cell lines with different endogenous SGPP1 levels consistently demonstrated that SGPP1 suppresses malignant ESCC cell behavior. SGPP1 overexpression inhibited the proliferation, migration and invasion of KYSE150 cells and promoted apoptosis, whereas SGPP1 knockdown enhanced these malignant phenotypes in ECA109 cells. Although SGPP1 participates in sphingolipid metabolism in other tumor contexts, the canonical SGPP1-S1P metabolic axis was not directly examined. Instead, subsequent transcriptomic and experimental analyses focused on identifying downstream regulatory molecules associated with SGPP1-mediated ESCC progression. SGPP1 has previously been identified as a negative regulator of malignant cell proliferation (19). With respect to metastatic properties, SGPP1 overexpression suppressed KYSE150 cell migration and invasion in wound-healing and Transwell assays, whereas SGPP1 knockdown enhanced the migratory and invasive potential of ECA109 cells. This finding is consistent with observations in GC, in which SGPP1 knockdown leads to S1P accumulation, a 2- to 5-fold increase in the migratory capacity of AGS and HGC27 cells, and a notable increase in invasive capacity (10). However, SGPP1 can exert an opposing role in certain cancers by promoting tumor progression. For instance, in glioma, SGPP1 knockdown markedly inhibited PAK1-induced glioma cell migration and resistance, indicating that SGPP1 cooperates with PAK1 to raise malignant tumor behavior (17). SGPP1 has also been reported to enhance oral cancer cell survival by regulating endoplasmic reticulum stress and autophagy; aberrant SGPP1 overexpression can raise the dedifferentiation of oral epithelial cells and thereby contribute to carcinogenesis (20). Thus, the function of SGPP1 appears to be highly context-dependent and can be influenced by the tumor microenvironment, cell type and upstream signaling pathways. Because the role of SGPP1 in ESCC has not previously been reported, further investigation of its tumor-suppressive mechanisms can facilitate the identification of novel therapeutic targets for this disease.

Identifying key regulators of metabolic reprogramming in ESCC is essential for understanding the limitations of current treatment strategies (21). A central finding of the present study is that SGPP1 can exert its effects through the regulation of UDP-glucuronosyltransferase (UGT)-mediated metabolic reprogramming. The KEGG pathways associated with downregulated DEGs were intersected with the GSEA-KEGG pathways using UpSet analysis to identify candidate downstream mediators of SGPP1. UGT1A9 and UGT2B28 were the only genes enriched across all overlapping downregulated pathways. TCGA-ESCC analysis revealed moderate inverse correlations between SGPP1 and UGT1A9/UGT2B28 at the mRNA level, whereas *in vitro* experiments demonstrated that SGPP1 negatively regulates the mRNA and protein expression of UGT1A9 and UGT2B28 in ESCC cells. UGT1A9 and UGT2B28 are members of the UGT superfamily, which comprises important phase II metabolic enzymes involved in the metabolism, inactivation and detoxification of endogenous and exogenous compounds through glucuronidation. Abnormal expression of these enzymes contributes to tumor metabolic reprogramming (22). UGT enzymes catalyze glucuronidation reactions and participate in drug metabolism, hormone inactivation and toxin elimination (22,23,24). Abnormal expression of UGT1A9 and UGT2B28 expression was associated with cancer progression and treatment response. In BC, resveratrol was reported to inhibit tumor cell proliferation by upregulating NRF2 and UGT1A9 expression, promoting estrogen metabolism *in vivo*, and reducing cellular damage caused by toxic estrogen metabolites (25). In patients with liver cancer treated with sorafenib after surgery, high UGT1A9 expression was associated with an improved prognosis, possibly because enhanced sorafenib glucuronidation improves treatment efficacy (26). UGT2B28 also affects steroid hormone metabolism in BC (27). In PC, UGT2B28 regulates steroid hormone metabolism and modulates testosterone and dihydrotestosterone levels. Elevated androgen levels upregulate UGT2B28, forming a feedback loop, and UGT2B28 can predict the risk and progression of PC (28). The findings of the present study link SGPP1 to UGT1A9/UGT2B28 and indicate that SGPP1 can alter the metabolic state of ESCC cells and suppress their growth and metastasis by inhibiting UGT-mediated metabolic pathways, including xenobiotic and retinol metabolism. These results expand the current understanding of the tumor-suppressive mechanisms of SGPP1 and the functions of the UGT family in ESCC.

From a clinical translational perspective, the findings of the present study suggest that SGPP1 may have prognostic value in ESCC. IHC demonstrated heterogeneous SGPP1expression in tumor tissues from 68 patients with ESCC, including 31 tumors with high SGPP1 expression and 37 with low SGPP1 expression. In this cohort, low SGPP1 expression remained significantly associated with poorer OS in the multivariable Cox model. Kaplan-Meier analysis further demonstrated that patients with high SGPP1 expression had a considerably longer OS than those with low SGPP1 expression. Collectively, these results support the clinical potential of SGPP1 as a candidate prognostic biomarker for ESCC, but the association should be interpreted cautiously pending validation in larger, independent cohorts.

A major strength of the present study is its comprehensive investigation of the biological functions and molecular mechanisms of SGPP1 in ESCC. Through the integration of *in vitro* cell experiments with clinical sample validation, UGT1A9 and UGT2B28 were identified for the first time as candidate downstream targets of SGPP1. The combined application of multiple bioinformatics approaches, including differential gene screening, GO, KEGG, GSEA and UpSet plots, together with experimental validation using western blotting, RT-qPCR and IHC, enhanced the robustness of the findings. Cox regression analysis suggested a potential prognostic association of SGPP1 in this cohort; however, this finding requires confirmation in larger independent cohorts.

Several limitations of the present study should be acknowledged. First, the clinical cohort used for the prognostic analysis of ESCC clinical samples was relatively small (n=68) and restricted to patients receiving radical radiotherapy, which limited statistical power and may have introduced selection

bias; therefore, larger multicenter clinical studies are required to validate the prognostic value of SGPP1. Second, the four overlapping downregulated KEGG pathways were all related to xenobiotic, drug, or retinoid metabolism, and UGT family members serve as shared phase II conjugating enzymes across these pathway annotations. This annotation structure can therefore increase the likelihood of identifying UGT genes at the intersection of all pathways. Third, the relationship between SGPP1 and UGT1A9/UGT2B28 was examined only at the mRNA and protein levels. The specific regulatory mechanisms underlying this relationship, including potential regulation through transcription factors or post-translational modifications, require further investigation. Fourth, only *in vitro* cell experiments were performed; therefore, *in vivo* studies, such as xenograft experiments in nude mice, are required to validate the tumor-suppressive effects of SGPP1 and the regulatory roles of UGT1A9/UGT2B28. Fifth, SGPP1 overexpression and knockdown were performed in only one ESCC cell line each (KYSE150 and ECA109, respectively). Although the reciprocal phenotypes support the functional role of SGPP1, cell-line-specific effects cannot be excluded, and validation in additional ESCC cell lines is warranted. Finally, SGPP1 knockdown efficiency was confirmed at both the mRNA and protein levels; however, only one siSGPP1 sequence was used. Although the loss-of-function phenotypes observed in ECA109 cells were directionally opposite to the gain-of-function phenotypes observed in KYSE150 cells, supporting the functional involvement of SGPP1 in ESCC cells, future studies using additional independent siRNAs or stable shRNA systems are required to strengthen the evidence for knockdown specificity. Moreover, the basal SGPP1 expression profile across ESCC cell lines shown in Fig. 1B was obtained as part of an exploratory cell-line screening experiment and was not quantitatively assessed in three independent biological replicates. Thus, the observed differences in basal SGPP1 protein expression among these cell lines should be interpreted qualitatively rather than as statistically validated quantitative differences.

The present study identified SGPP1 as a tumor suppressor in ESCC. SGPP1 negatively regulates UGT1A9 and UGT2B28 expression, modulates ECM remodeling and xenobiotic metabolic pathways, inhibits ESCC cell proliferation, migration and invasion, and increases apoptosis-associated DNA fragmentation. Low SGPP1 expression is associated with poor prognosis in this cohort and may have value as a prognostic biomarker. These findings broaden the current understanding of the molecular mechanisms underlying ESCC progression and provide a rationale for further evaluation of SGPP1 as a diagnostic, prognostic and therapeutic target.

Acknowledgements

Not applicable.

Funding

The present study was supported by the Hebei Natural Science Foundation (grant no. H2022206572), the Medical Science Research Project of Hebei (grant no. 20250042) and the Hebei Medical-Research-Enterprise Joint Innovation Special Project Program (grant no. LH20250063).

Availability of data and materials

The data generated in the present study may be requested from the corresponding author.

Authors' contributions

LS, LH and XH conceived and conducted the experiments, analyzed the data, prepared the figures and/or tables, and drafted and/or verified the manuscript. GZ, JL, YW and YH contributed to data analysis and manuscript revision. HZ designed the experiments and drafted or critically reviewed the manuscript. XX supervised the whole study and critically revised the manuscript. HZ and XX confirm the authenticity of all the raw data. All authors read and approved the final version of the manuscript.

Ethics approval and consent to participate

All procedures involving human participants were conducted in accordance with the 1964 Declaration of Helsinki and its subsequent amendments and with the ethical standards of the institutional research committee. The study was approved by the Ethics Committee of The Second Hospital of Hebei Medical University (approval no. 2024-R393; Shijiazhuang, China), and written informed consent was obtained from all participants.

Patient consent for publication

Not applicable.

Competing interests

The authors declare that they have no competing interests.

Use of artificial intelligence tools

During the preparation of this work, artificial intelligence tools were used to improve the readability and language of the manuscript or to generate images, and subsequently, the authors revised and edited the content produced by the artificial intelligence tools as necessary, taking full responsibility for the ultimate content of the present manuscript.

References

1. Bray F, Laversanne M, Sung H, Ferlay J, Siegel RL, Soerjomataram I and Jemal A: Global cancer statistics 2022: GLOBOCAN estimates of incidence and mortality worldwide for 36 cancers in 185 countries. CA Cancer J Clin 74: 229-263, 2024.
2. Yang J, Nie J, Xing S, Jiang K and Huang A: Minimally invasive resection of synchronous esophageal cancer and giant thymoma: A case report. Oncol Transl Med: July 9, 2025 (Epub ahead of print).
3. Lyu G and Li D: ZNF165: A pan-cancer biomarker with prognostic and therapeutic potential. Protein Pept Lett 32: 206-223, 2025.
4. Hou L, Hao Z, Zhang G, Li J, Wang Y, Xue X and Zhou H: CD9 regulates proliferation, invasion, migration and radioresistance of esophageal squamous cell carcinoma by activating AKT/GSK3β signaling pathway. Front Oncol 15: 1625120, 2025.
5. Han B, Zheng R, Zeng H, Wang S, Sun K, Chen R, Li L, Wei W and He J: Cancer incidence and mortality in China, 2022. J Natl Cancer Cent 4: 47-53, 2024.

6. Pan S, Hao Y, Ke Y, Zhang R, Zhao X, Ma X, Guo W, Wang X and Ma H: Albumin-to-globulin ratio as a prognostic indicator in elderly patients with esophageal squamous cell carcinoma undergoing radical radiotherapy. Oncol Transl Med 12: 101-107, 2026.
7. Yi Y, Cao Q, Zhang H, Zhang B, Zhang R, Li X, Kong L and Li B: Efficacy of neoadjuvant chemoimmunotherapy in locally advanced resectable esophageal cancer. J Cancer Res Ther 21: 934-940, 2025.
8. Zhao YX, Zhao HP, Zhao MY, Yu Y, Qi X, Wang JH and Lv J: Latest insights into the global epidemiological features, screening, early diagnosis and prognosis prediction of esophageal squamous cell carcinoma. World J Gastroenterol 30: 2638-2656, 2024.
9. Jiang H, Jin X, Gu H, Li B, Li Z and Sun Y: SPC25 upregulates CCND1 to promote the progression of esophageal squamous cell carcinoma by inhibiting MDM2-mediated E2F1 ubiquitination. Transl Oncol 53: 102300, 2025.
10. Gao XY, Li L, Wang XH, Wen XZ, Ji K, Ye L, Cai J, Jiang WG and Ji JF: [Corrigendum] Inhibition of sphingosine-1-phosphate phosphatase 1 promotes cancer cells migration in gastric cancer: Clinical implications. Oncol Rep 39: 2051, 2018.
11. Sattar RSA, Sumi MP, Nimisha, Apurva, Kumar A, Sharma AK, Ahmad E, Ali A, Mahajan B and Saluja SS: S1P signaling, its interactions and cross-talks with other partners and therapeutic importance in colorectal cancer. Cell Signal 86: 110080, 2021.
12. Ogretmen B: Sphingolipid metabolism in cancer signalling and therapy. Nat Rev Cancer 18: 33-50, 2018.
13. Zhao J, Tian XC, Zhang JQ, Li TT, Qiao S and Jiang SL: Tribulus terrestris L. induces cell apoptosis of breast cancer by regulating sphingolipid metabolism signaling pathways. Phytomedicine 120: 155014, 2023.
14. Nema R and Kumar A: Sphingosine-1-phosphate catabolizing enzymes predict better prognosis in triple-negative breast cancer patients and correlates with tumor-infiltrating immune cells tumor-infiltrating immune cells. Front Mol Biosci 8: 697922, 2021.
15. Huang X, Taeb S, Jahangiri S, Emmenegger U, Tran E, Bruce J, Mesci A, Korpela E, Vesprini D, Wong CS, *et al*: miRNA-95 mediates radioresistance in tumors by targeting the sphingolipid phosphatase SGPP1. Cancer Res 73: 6972-6986, 2013.
16. He J, Zhao H, Liu X, Wang D, Wang Y, Ai Y and Yang J: Sevoflurane suppresses cell viability and invasion and promotes cell apoptosis in colon cancer by modulating exosome-mediated circ-HMGCS1 via the miR-34a-5p/SGPP1 axis. Oncol Rep 44: 2429-2442, 2020.
17. Kim JH, Seo Y, Jo M, Jeon H, Kim YS, Kim EJ, Seo D, Lee WH, Kim SR, Yachie N, *et al*: Interrogation of kinase genetic interactions provides a global view of PAK1-mediated signal transduction pathways. J Biol Chem 295: 16906-16919, 2020.
18. Livak KJ and Schmittgen TD: Analysis of relative gene expression data using real-time quantitative PCR and the 2(-Delta Delta C(T)) method. Methods 25: 402-408, 2001.
19. Petrusca DN, Mulcrone PL, Macar DA, Bishop RT, Berdyshev E, Suvannasankha A, Anderson JL, Sun Q, Auron PE, Galson DL and Roodman GD: GFI1-dependent repression of SGPP1 increases multiple myeloma cell survival. Cancers (Basel) 14: 772, 2022.
20. Vishwakarma S, Joshi D, Pandey R, Das S, Mukhopadhyay S, Rai R, Singhal R, Kapoor N and Kumar A: Downregulation of lipid phosphate phosphatase 3 correlates with tumor-infiltrating immune cells in oral cancer. Cureus 14: e23553, 2022.
21. Zhang GC, Yu XN, Guo HY, Sun JL, Liu ZY, Zhu JM, Liu TT, Dong L, Shen XZ and Yin J: PRP19 enhances esophageal squamous cell carcinoma progression by reprogramming SREBF1-dependent fatty acid metabolism. Cancer Res 83: 521-537, 2023.
22. Liu W, Li J, Zhao R, Lu Y and Huang P: The uridine diphosphate (UDP)-glycosyltransferases (UGTs) superfamily: The role in tumor cell metabolism. Front Oncol 12: 1088458, 2023.
23. Stresser DM and Zientek MA: UDP-Glucuronosyl transferase mediated drug-drug interactions: An Industry perspective on recommended in vitro studies. Drug Metab Pharmacokinet 67: 101526, 2026.
24. Zeng X, Jiang W, He B, Li L, Wu T, Fu F, Yao H, Liao G, Wang C and Wu D: Tissue-derived extracellular vesicles-mediated delivery of a hepatic enzyme living panorama (HELP) for treating multifactorial liver diseases. J Nanobiotechnology 24: 310, 2026.
25. Thibaudeau J, Lépine J, Tojcic J, Duguay Y, Pelletier G, Plante M, Brisson J, Têtu B, Jacob S, Perusse L, *et al*: Characterization of common UGT1A8, UGT1A9, and UGT2B7 variants with different capacities to inactivate mutagenic 4-hydroxylated metabolites of estradiol and estrone. Cancer Res 66: 125-133, 2006.
26. Ge Y, Chen S, Mu W, Ba Q, Li J, Chen P, Wang X and Wang H: Epigenetic regulation of UDP-Glucuronosyltransferase by microRNA-200a/-183: Implications for responses to sorafenib treatment in patients with hepatocellular carcinoma. Cancer Lett 454: 14-25, 2019.
27. Cao Q, Chen X, Wu X, Liao R, Huang P, Tan Y, Wang L, Ren G, Huang J and Dong C: Inhibition of UGT8 suppresses basal-like breast cancer progression by attenuating sulfatide-αVβ5 axis. J Exp Med 215: 1679-1692, 2018.
28. Belledant A, Hovington H, Garcia L, Caron P, Brisson H, Villeneuve L, Simonyan D, Têtu B, Fradet Y, Lacombe L, *et al*: The UGT2B28 sex-steroid inactivation pathway is a regulator of steroidogenesis and modifies the risk of prostate cancer progression. Eur Urol 69: 601-609, 2016.

Copyright © 2026 Su et al. This work is licensed under a Creative Commons Attribution-NonCommercial 4.0 International (CC BY-NC 4.0) License.